Journal of Fluids and Structures (1987) **1**, 381–399

THE RELATIONSHIP BETWEEN IN-LINE AND CROSS-FLOW VORTEX-INDUCED VIBRATION OF CYLINDERS

J. K. VANDIVER

Department of Ocean Engineering, Massachusetts Institute of Technology, Cambridge, Massachusetts 02139, U.S.A.

AND

J.-Y. JONG

Wyle Laboratories, Huntsville, Alabama, U.S.A.

(Received 10 September 1986 and in revised form 30 January 1987)

Cable strumming experiments were conducted at Castine, Maine in 1981 and from an icebreaker in 1983. The purpose was to study the vibration characteristics of long flexible cylinders subjected to vortex-induced oscillation. Particular emphasis was placed on the investigation of the relationship between in-line and cross-flow vibration. Under non-lock-in, random vibration conditions, linear spectral analysis indicated that in-line and cross-flow response were linearly independent of each other, while the results of modal analysis showed that the moving average vibration energies in these two directions were strongly related. A higher order spectral analysis was performed to demonstrate a non-linear correlation between in-line and cross-flow vibration of flexible cylinders excited by vortex shedding in both uniform flow and sheared flow conditions.

The results of bispectral analysis demonstrated the existence of a quadratic relationship between in-line and cross-flow motion under both lock-in and non-lock-in conditions. The well-known frequency doubling phenomena in in-line response was proven to be the result of such a quadratic correlation.

INTRODUCTION

MANY TYPES of ocean-based structures, such as marine risers, TLP tension members, deep water pipelines and hydrophone cables are susceptible to vortex-induced vibration. These strumming oscillations are of great practical importance because they may cause failure by fatigue.

The resolution of problems associated with prediction of vortex-induced vibration has proven to be extremely difficult, due to the complex, non-linear interactions between the structural motions and the vortex-shedding. The well-known wake capture phenomenon is a typical example of such non-linear interactions. A sampling of papers on this topic can be found in References [1]–[4].

The emphasis in the literature has been placed mostly on the study of vibration characteristics in the cross-flow direction. The behavior in the in-line direction is much less well understood. No attempt has been made previously to investigate the relationship between cross-flow and in-line response, or equivalently, between lift and drag forces under non-lock-in conditions. Even the answer to the preliminary question of whether

0889–9746/87/040381 + 19 $03.00/0

they are correlated or independent is not available for non-lock-in conditions. In the design of, for example, a marine riser, the correlation between the response in these two perpendicular directions plays an important role in fatigue life estimation, because of its relation to the stress statistics of the structure.

One of the purposes of the experiments described in this paper was to study the relationship between in-line and cross-flow response of long flexible cylinders under realistic field conditions. These tests were more realistic than laboratory ones, because it was possible to use cylinders of sufficient length so that many different natural modes could be excited, simultaneously, in both directions. The experiments at Castine were performed on flexible cylinders, 75 ft (22·86 m) long, which were exposed to a uniform current. Measurements taken included current, drag, tension, and biaxial acceleration at seven locations unequally spaced along the test cylinder. Linear spectral analysis of lock-in and non-lock-in response data revealed little coherence between in-line and cross-flow vibration.

A frequency doubling relationship between cross-flow and in-line response has long been observed for lock-in conditions and has been evident in an approximate sense in the broad-band spectral characteristics typical of multi-moded non-lock-in conditions. Quadratic operations are known to have frequency doubling characteristics.

Furthermore, by a least squares error-minimization method, it was possible to evaluate the individual modal contributions for in-line and cross-flow motions under lock-in and non-lock-in conditions, thus enabling the computation of vibration energy. The results of modal analysis showed that there existed a strong correlation between the drag coefficient and the total vibration energy as well as a correlation between the in-line and cross-flow vibration energy. The evidence suggested that a spectral analysis technique capable of detecting quadratic system behavior was required. Bispectral analysis is specifically sensitive to quadratic relationships. The cross-bicoherence spectrum ultimately provided definitive evidence of a quadratic correlation between cross-flow and in-line response under both lock-in and non-lock-in conditions.

In linear spectral estimation the assumption is made that two different frequency components in the same or different time series are independent of one another. Therefore, if one computes the coherence between a sinusoidal signal and the square of the same time series, the result is zero at all frequencies. This is because the process of squaring generates a new time series, which has as its principal frequency component a sinusoid at twice the original frequency. This can be proven by simple trigonometric identities for sine squared. The squaring process is nonetheless explicitly deterministic and there must be a phase relationship between the two time series. Linear coherence function analysis is incapable of revealing such correlations.

Quadratic operations are ones which involve squares or products of variables in an equation or in times series. The bispectrum and the bicoherence are capable of revealing such quadratic correlations. The bispectral estimator is nothing more than the expected value of the product of three different Fourier coefficients which are computed by an FFT. For example, the ensemble average of many independent computations of the product between the ith, jth and $(i+j)$th Fourier coefficients will be zero, unless the $(i+j)$th component is phase-related to the i and j components. This would be the case if the $i+j$ component had been generated by a product of terms involving the frequencies at i and j. It will be shown in this paper that numerous quadratic relationships exist between the in-line and cross-flow motions produced by vortex-induced lift and drag forces.

These conclusions are verified using data gathered at the experimental site in Castine, Maine, and on very long cables deployed in sheared currents under the ice in the Arctic in 1983.

THE EXPERIMENTS

CASTINE—1981

The site chosen for the experiment was a sand-bar located at the mouth of Holbrook Cove near Castine, Maine. At low tide, the sand-bar was exposed, allowing easy access to the test equipment, while at high tide it was covered by about 10 ft (3 m) of water. The test section was oriented normal to the direction of the current which varied from 0 to 2·4 ft/s (0·73 m/s) over the tidal cycle with only small spatial differences over the section length at any given moment. The data-taking station for the experiment was the R/V Edgerton, moored approximately 300 ft (91·5 m) from the sand-bar and chartered from the MIT Sea Grant Program. Figure 1 shows a schematic diagram of the test section.

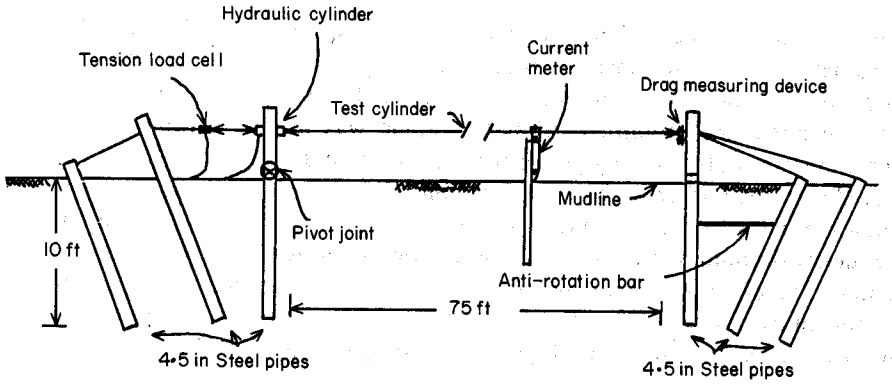

Figure 1. Schematic diagram of the experiment test section.

A 75 ft (22·86 m) long instrumented cable was developed specifically for this experiment. The outer sheath for the cable was a single piece of clear flexible PVC tubing, which had an outer diameter of $1\frac{1}{4}$ in (3·18 cm) and an inner diameter of 1·0 in (2·54 cm). Three $\frac{1}{8}$ in diameter stainless steel cables ran through the tubing and served as tension-carrying members. Seven biaxial pairs of accelerometers were placed along the cable at positions L/8, L/6, L/4, 2L/5, 5L/8, and 3L/4, where L is the length of the cable. The accelerometers were Sundstrand Mini-Pal Model 2180 Servo Accelerometers, which are sensitive to the direction of gravity. The biaxial pairing of these accelerometers made it possible to determine their orientation and hence extract real vertical (cross-flow) and horizontal (in-line) accelerations of the cable at the seven locations. For some tests the composite cable was placed inside a steel tube of outer diameter 1·631 in (4·14 cm) and inner diameter 1·493 in (3·79 cm), referred to as the pipe.

A load cell mounted at one end of the test cylinder measured the horizontal shear force on one end of the test cylinder. The cylinder and its two end supports were symmetric, and therefore the measured force was one half the total drag force on the cylinder. Mean drag force was measured. The load cell was a Sensotec Model 41, packaged for underwater use. The current was measured by a Neil Brown Instrument Systems DRCM-2 Acoustic Current Meter located 12·5 ft (3·66 m) from the west end of the test cylinder and 2 ft upstream. It was set so that it determined the current at the level of the test cylinders. The current was found to be spatially uniform to within 3·0% from end to end for all current speeds above 0·5 ft/s (0·15 m/s). Additional details can be found in References [5]–[7].

THE ARCTIC—1983

During an Arctic cruise in the summer of 1983 on the Research Vessel *Polarstern*, cable strumming experiments were conducted in sheared currents near the ice edge in the Frahm Strait close to the eastern coast of Greenland. The cables, up to 2000 ft (610 m) long, were suspended vertically under the ice and provided data with hundreds of modes responding simultaneously. Current profiles were recorded using the same acoustic current meter, and acceleration was measured using biaxial pairs of piezoelectric accelerometers. For complete details see References [8] and [9].

PRELIMINARY ANALYSIS OF THE DATA FROM CASTINE

DETERMINATION OF DISPLACEMENT RESPONSE AND DRAG COEFFICIENTS

The orientation of the biaxial accelerometers was initially unknown. However, the accelerometers used were sensitive to gravity and gave a DC offset to the recorded signal in proportion to the vector component of gravity. From the DC offset the accelerometer orientation angle was obtained. After this angle was found, the in-line and cross-flow accelerations were obtained by performing a vector rotation.

Once the in-line and cross-flow accelerations were found, it was necessary to undertake a complex process to determine the displacement-time histories by double integration. In the frequency domain, the transfer function of an integrator possesses a singularity at zero frequency. Therefore, low frequency noise components near this singularity blow up and smear the output signal from the integrator. To avoid this, an effective filtering and integration procedure was developed. The details may be found in the thesis by Jong [10].

A broad view of the data may be obtained by examining compressed 2½ h records of drag coefficient, current speed, and r.m.s. displacement response as shown in Figure 2. Data was collected on the rising tide. This example represents one complete experimental run.

The data shown were calculated by a moving average whose window was 8·53 s in length, which is long enough to average over many cycles of vibration, but short enough

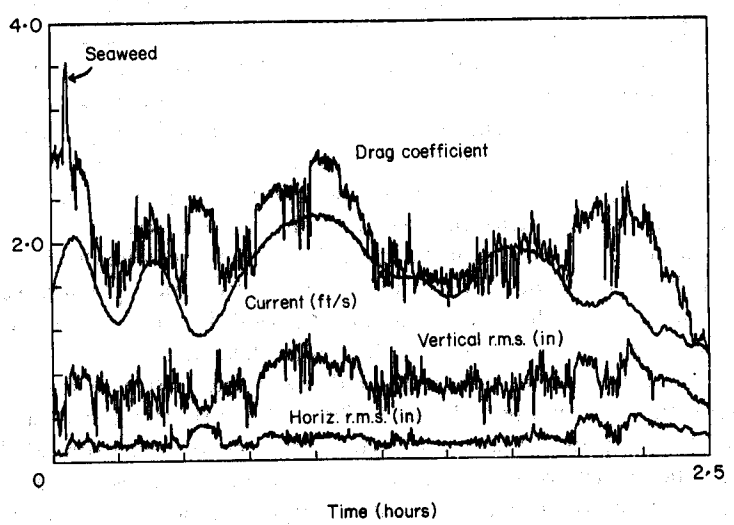

Figure 2. Moving average record of the r.m.s. displacement at L/8, current, and drag coefficient for the pipe.

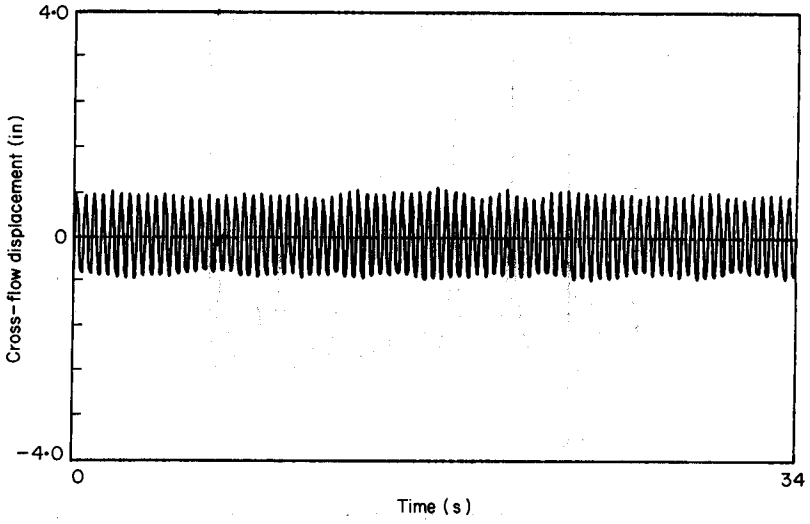

Figure 3. Cross-flow displacement at lock-in.

to show subtle variations in behavior. The displacement data were taken from location L/6. Over the $2\frac{1}{2}$ h span of time shown in the figure, some periods correspond to lock-in response, and others to non-lock-in. As the current speed fell within a lock-in range, a substantial increase of cross-flow and/or in-line r.m.s. displacement was apparent. A corresponding elevated plateau in the drag coefficient is also observed. These are raw r.m.s. displacements at the location specified and have not been corrected for mode shape. Due to the fact that these raw data are highly positional and mode shape dependent, the in-line and cross-flow r.m.s. displacements in the figure do not give a good indication of any relationship existing between the two. A modal analysis is required to represent the behavior of the entire cylinder and to understand the relationship between in-line and cross-flow motion. It is instructive to begin with sample time histories typical of lock-in and non-lock-in behavior.

Response Characteristics under Lock-in Conditions

Lock-in occurs when the vortex shedding frequency falls within a few percent of a natural frequency of the cylinder. The vortex shedding process is synchronized with the cylinder motion, and a stable, periodic, transverse displacement of nearly constant amplitude is observed. Figure 3 shows an example of a cross-flow displacement time-history of the pipe at L/4 during lock-in with the third mode. Figure 4 is the corresponding acceleration power spectrum, presented on a logarithmic scale. The dominant response peak is at 2·4 Hz. All spectra shown in this paper were computed using a 100-pole maximum entropy spectral estimator [11]. The input was an autocorrelation function 34 s in maximum lag, computed from 136 s of data. The sampling rate was 30 Hz.

In the in-line direction, the motion is quite different. A periodic displacement of non-constant amplitude is apparent in Figure 5. Figure 6 presents the corresponding acceleration power spectrum. One important observation in this result is that the dominant frequency in the in-line direction is 4·8 Hz, exactly double that in the cross-flow direction. This frequency doubling phenomenon was always observed under lock-in conditions.

By double integration of both measured in-line and cross-flow acceleration time-histories, it is possible to plot the trajectory of the motion of a point on the cylinder.

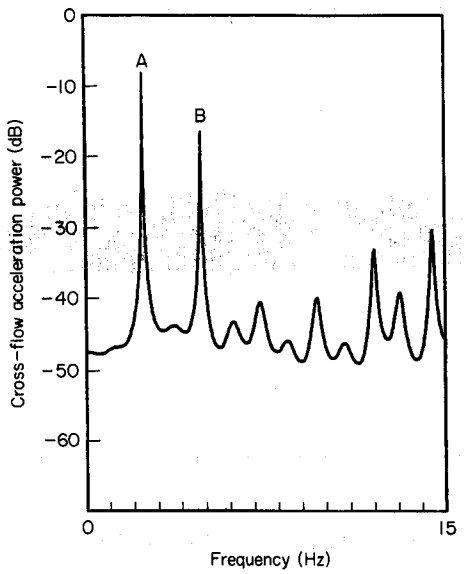

Figure 4. Acceleration spectrum of cross-flow response at lock-in. $f_A = 2{\cdot}4$ Hz; $f_B = 4{\cdot}8$ Hz.

Figure 7 shows the motion at L/4 projected onto a plane which is normal to the cylinder axis (orbital diagram). This point on the pipe prescribed figure-of-eight motions. In this case the cross-flow motion resulted from lock-in of the third mode at a frequency of 2·4 Hz. The in-line motion was primarily at twice the frequency of the cross-flow motion and was dominated by response in the fifth mode. The fifth mode natural frequency for this cylinder is twice that of the third mode. Though at different frequencies the two motions must be highly correlated.

At this point in the analysis, one does not generally know for certain which natural modes of vibration are responding. It will in fact be shown that the in-line response, though sharply peaked at one frequency, does not always correspond to a resonant

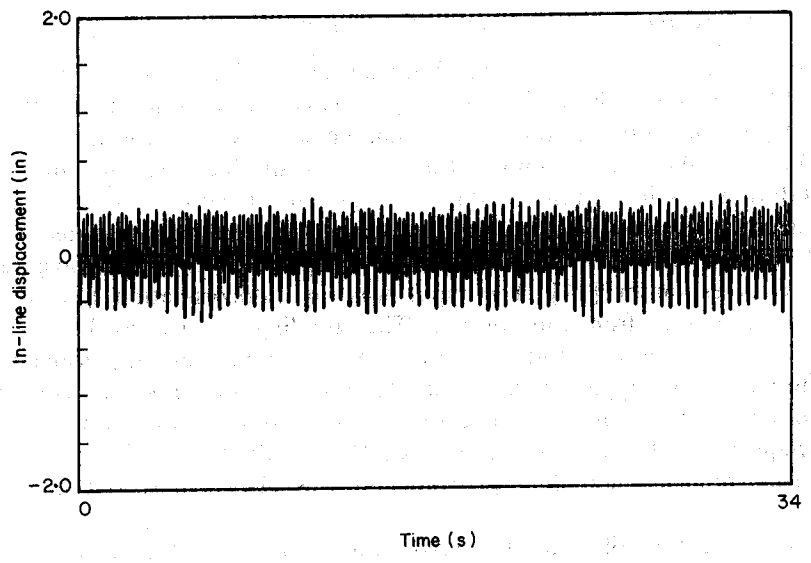

Figure 5. In-line displacement at lock-in.

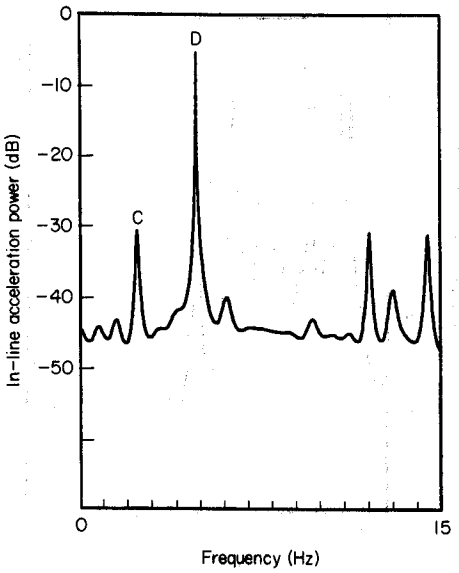

Figure 6. Acceleration spectrum of in-line response at lock-in. $f_C = 2{\cdot}4$ Hz; $f_D = 4{\cdot}8$ Hz.

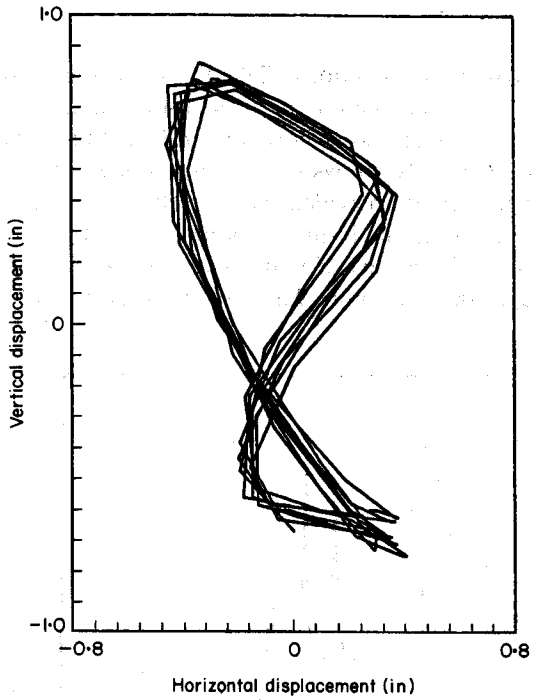

Figure 7. Orbital motion at L/4 at lock-in.

natural frequency, as it does in this case. Under lock-in conditions it is always at twice the cross-flow lock-in frequency.

Response Characteristics under Non-lock-in Conditions

When the vortex shedding frequency is outside of the lock-in range, non-lock-in vibration results. The response is characterized by random fluctuations of amplitude and frequency

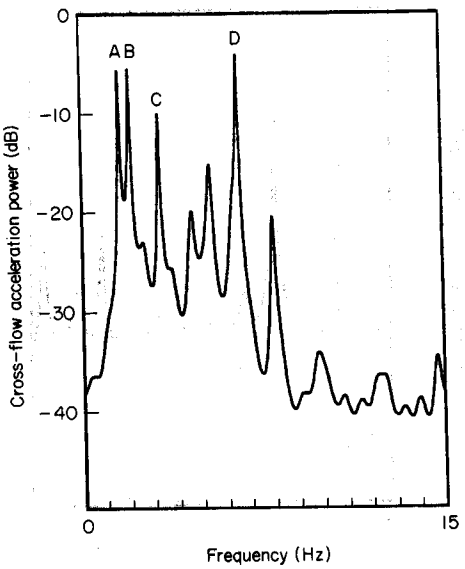

Figure 8. Power spectrum of cross-flow acceleration at non-lock-in. $f_A = 1{\cdot}70$ Hz; $f_B = 2{\cdot}00$ Hz; $f_C = 3{\cdot}20$ Hz; $f_D = 6{\cdot}40$ Hz.

in both in-line and cross-flow directions. The lift force correlation length along the cylinder becomes much shorter than that at lock-in. Figures 8 and 9 show typical acceleration power spectra in the cross-flow and in-line directions. Wide band lift and drag forces are implied. Figure 10 shows the corresponding orbital diagram; the random walk character of the figure gives no evidence of correlation. An important observation to be made is that spectral peaks in the in-line response occur at frequencies which are equal to the sums of various combinations of two spectral peak frequencies in the cross-flow direction. For example, peak E in Figure 9 at 3·70 Hz is the sum of 1·70 and 2·00 Hz from

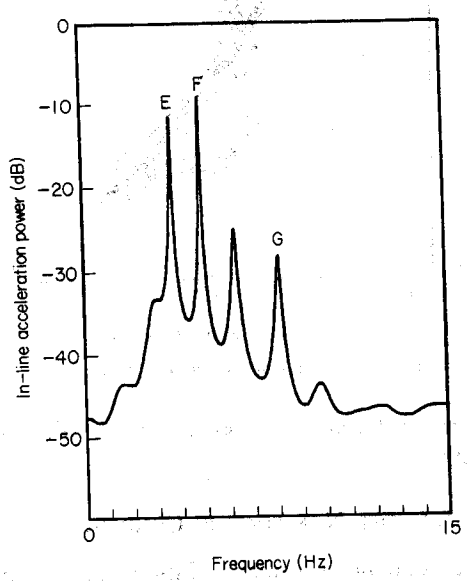

Figure 9. Power spectrum of in-line acceleration at non-lock-in. $f_E = 3{\cdot}70$ Hz; $f_F = 4{\cdot}90$ Hz; $f_G = 8{\cdot}10$ Hz.

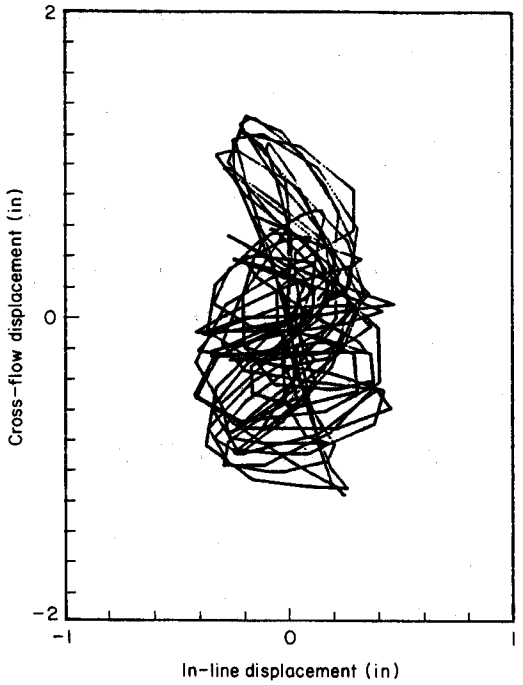

Figure 10. Orbital motion at L/8 at non-lock-in.

peaks A and B. Peak F in Figure 9 is at 4·9 Hz which, not coincidentally, is the sum of the frequencies of the peaks A and C in the cross-flow spectrum shown in Figure 8. The frequency doubling and summing phenomena seen in the lock-in and non-lock-in data suggest non-linear quadratic correlation. Furthermore, linear coherence between displacements in the two directions is very low [10, 12]. In-line response peaks for both lock-in and non-lock-in cases frequently do not correspond to natural frequencies. The subject of which modes account for this response is an interesting one and will be discussed in the next section.

MODAL ANALYSIS

In this section, a least squares error minimization method is used to estimate the modal displacements of all the participating modes. Vibration energies in both directions are then calculated from the modal displacements and the known mode shapes. By this method of modal analysis, the response of the cylinder can be expressed in terms of a superposition of mode shapes $Y_i(x)$ multiplied by the modal displacements $P_i(t)$ [10, 13], i.e.

$$y(x, t) = \sum_i P_i(t) Y_i(x). \tag{1}$$

In this experiment, the response was measured at seven unequally spaced positions. A least squares method was used to estimate the modal displacement time histories in terms of the measured responses at these seven positions. For each test case the response was dominated by a finite number of modes, usually two to six in number. A first guess at the responding modes was obtained by inspection of the response spectrum at any one location. By summing the normal mode responses over the apparent participating modes, the following equations are obtained, where the range M to N covers all of the

participating modes. For taut, constant tension, pin-supported, uniform cylinders, the ith mode shape is given by a sinusoidal curve as

$$Y_i(x) = \sin(i\pi x/L). \tag{2}$$

At time $t = t_0$, the response of position $x = x_j$ can be expressed as

$$y(x_j, t_0) = \sum_{i=M}^{N} P_i(t_0) Y_i(x_j) + E(x_j), \tag{3}$$

where $E(X_j)$ is the error term. Rewriting equation (3) in matrix form,

$$\{y\} = [Y]\{P\} + \{E\}, \tag{4}$$

where

y_j is an element in the vector of the measured response at t_0,
Y_{ij} is an element in the mode shape matrix,
P_i is an element in the vector of the natural coordinates at t_0,
E_j is the error vector,

and $i = M, N, j = 1, 7$.

The sum of error squares, ee, is given by

$$\begin{aligned} \text{ee} &= \{E\}^T\{E\} = (\{y\} - [Y]\{P\})^T(\{y\} - [Y]\{P\}) \\ &= \{y\}^T\{y\} - 2\{P\}^T[Y]^T\{y\} + \{P\}^T[Y]^T[Y]\{P\}. \end{aligned} \tag{5}$$

The vector of natural coordinates P_i is to be determined such that the error squared term is minimized,

$$\min[\text{ee}] = \min[\{E\}^T\{E\}]. \tag{6}$$

Let

$$\frac{\mathrm{d}(\text{ee})}{\mathrm{d}P_i} = 0, \tag{7}$$

and solve for $P(t)$, i.e.

$$\{P\} = [[Y]^T[Y]]^{-1}[Y]^{-1}\{y\}, \tag{8}$$

or

$$\{P\} = [T]\{y\}, \tag{9}$$

where $[T]$ is the transfer matrix

$$[T] = [[Y]^T[Y]]^{-1}[Y]. \tag{10}$$

Equation (9) decomposes the measured response at the seven positions into the natural coordinates, provided the mode shapes are known and the guess of the responding modes is initially correct. Figure 11 shows an example of the in-line pipe displacement at position L/8. In the displacement spectrum, there are several peaks, each likely corresponding to one particular mode to be identified. Using the method discussed above, the natural coordinate time histories were obtained for the 4th, 5th, 6th, and 7th modes. These modal displacement time-histories are shown in Figure 12. Each time-history represents an antinode displacement for that mode expressed in inches. A scale of -1 to $+1$ in is shown on the Figure. All modal time-histories are to be considered to have a zero mean. Their sum, correctly weighted by the value of the respective mode shapes at any particular location, would equal the displacement at that point.

At constant current speed, when the cylinder is at non-lock-in, the participation of different contributing modes varies with time as illustrated in Figure 12. It is enlightening to study this feature of non-lock-in response on a longer time scale. A 448 s record of non-lock-in pipe response was analyzed and the contributing modal displacements were evaluated. Moving average r.m.s. modal displacement responses in both directions were

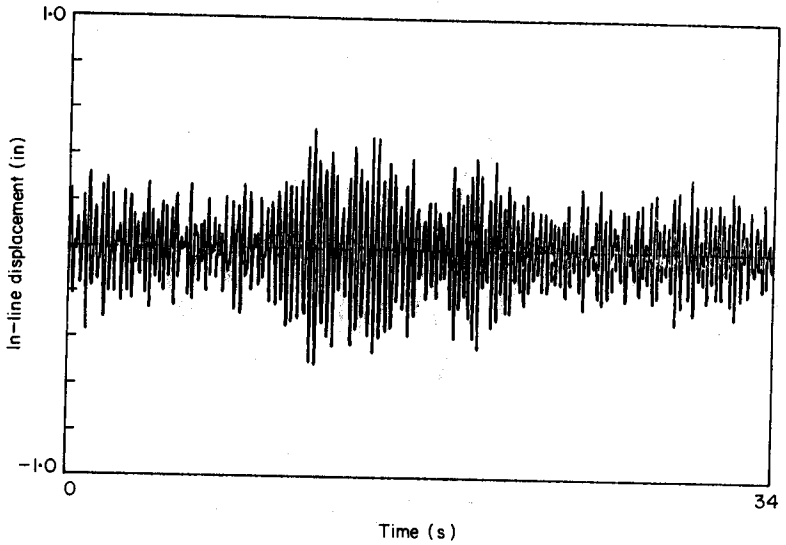

Figure 11. In-line displacement at L/8 at non-lock-in; 4th, 5th, 6th, and 7th modes responding.

calculated. These are plotted (in inches) in Figures 13 and 14. The r.m.s. value of the individual modal antinode responses are shown. Notice that as the response of one mode recedes, another appears to take its place.

The amplitude scales on Figures 13 and 14 are to be interpreted as follows. Each modal r.m.s. amplitude is plotted above a horizontal line representing zero deflection for that mode. If the scale given on the left edge of the Figure and spanning 0 to 2·0 in (5·08 cm) is moved upwards until zero corresponds to the zero line for the mode of interest, then the response can be read-off directly. For example, the maximum r.m.s. response for mode 2 is approximately 0·72 in (1·83 cm).

The same graphical scaling method is used in Figure 15, except that the units of energy are ft lb and of current speed are ft/s. The drag coefficient is dimensionless.

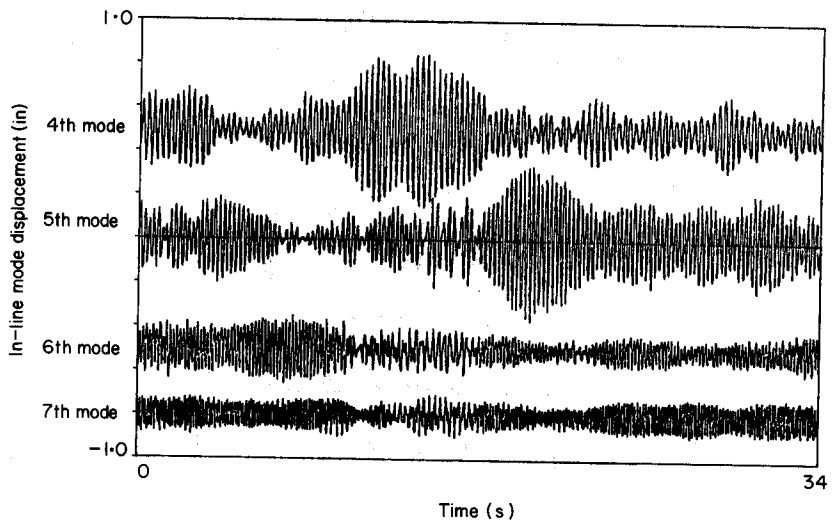

Figure 12. Natural coordinate time-histories for the 4th, 5th, 6th, and 7th in-line modes of the pipe.

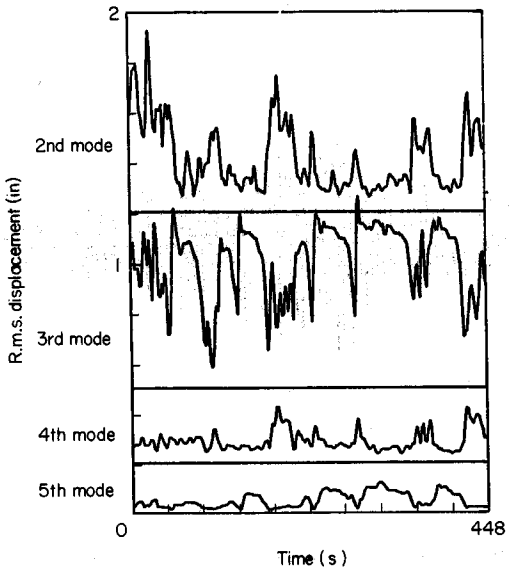

Figure 13. Natural coordinate r.m.s. displacements for the 2nd, 3rd, 4th, and 5th cross-flow modes of the pipe.

Moving average vibration energies were calculated from these natural coordinates and mode shapes in both in-line and cross-flow directions as shown in Figure 15. The vibration energy is given by

$$E(t) = \tfrac{1}{4}L\sum_i [EIP_i^2(t)(i\pi/L)^4 + TP_i^2(i\pi/L)^2 + m\dot{P}_i^2(t)], \tag{11}$$

where the dot denotes differentiation with respect to t. Obvious correlations exist between in-line and cross-flow vibration energy and between vibration energy and drag coefficient, as can be seen in Figure 15. The high plateaus in drag coefficient and response energy

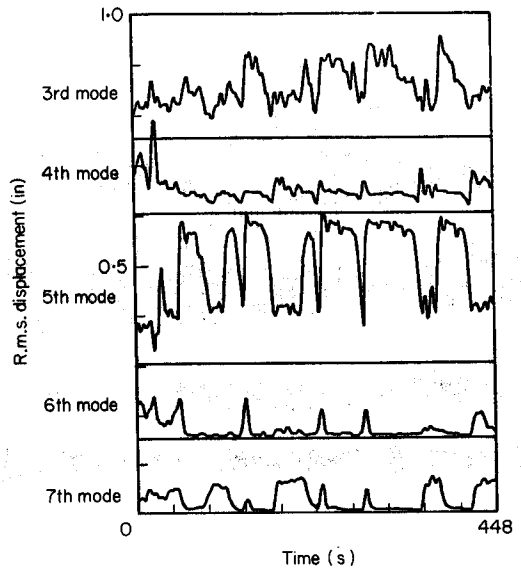

Figure 14. Natural coordinate r.m.s. displacements for 3rd, 4th, 5th, 6th, and 7th in-line modes of the pipe.

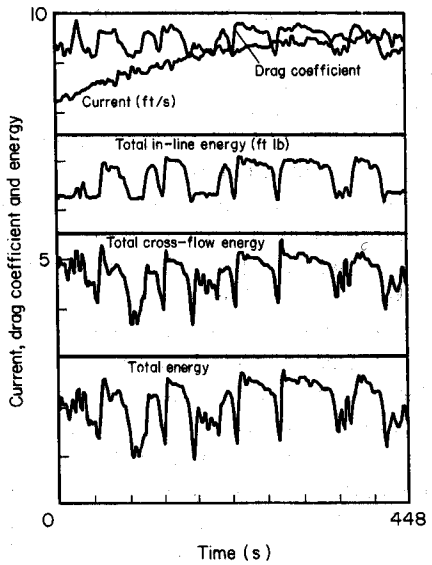

Figure 15. Current velocity (ft/s) drag coefficient, and vibration energy (ft lbf).

correspond to periods when one mode was able to dominate the response, and lock-in or partial lock-in over a portion of the cylinder existed. This figure represents flow conditions at the boundary between lock-in and non-lock-in behavior. A scatter diagram of the in-line vibration energy *versus* drag coefficient is plotted in Figure 16. The temporal history is retained by connecting successive points as indicated by the arrows. A very clear

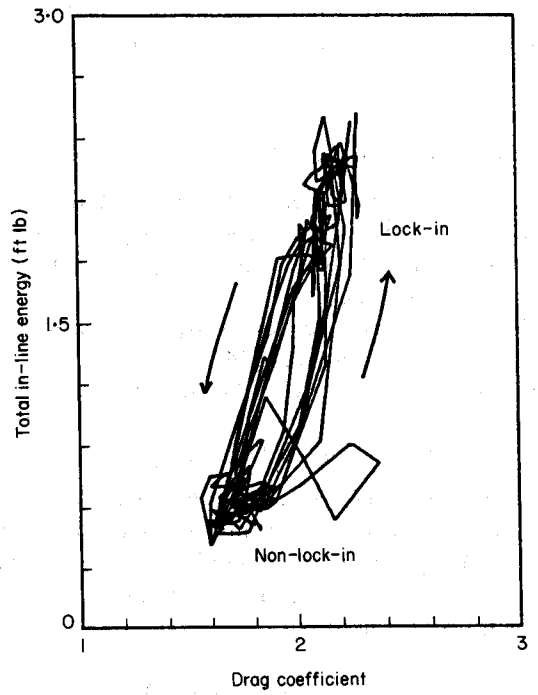

Figure 16. Drag coefficient *versus* total in-line vibration energy.

memory phenomenon is revealed. Drag coefficients are higher while going into lock-in than coming out.

As mentioned before, the in-line response frequencies are equal to the sums of pairs of cross-flow response frequencies. It is usually not obvious which in-line modes respond. Modal identification methods were used to provide the answer, with some very surprising results. One interesting case is described below.

For a taut cable, all of the natural frequencies are integer multiples of the lowest. Therefore, under lock-in conditions, it is reasonable to expect that the fluctuating drag forces will excite an in-line mode whose natural frequency is twice that of the mode which is responsible for the cross-flow lock-in. This is not always the case, however, as will be shown. In the example, a modal analysis of data taken with the bare cable revealed that the cross-flow vibration was a second-mode lock-in. It was expected that the unsteady drag forces would excite the fourth in-line mode, because its natural frequency was the same as the drag force fluctuations. However, modal analysis revealed that in-line motion was in the third mode, instead of the fourth mode as had been expected. The frequency of this third motion was not the natural frequency of the third mode, but was in fact equal to the natural frequency of the fourth mode. The response was not resonant with the fourth mode, but was an inertia-controlled response of the third mode.

Though not initially obvious, the explanation is quite simple and applies to all taut cables and pipes with sinusoidal mode shapes. Under lock-in conditions the shedding of vortices over the entire cylinder is essentially simultaneous, independent of the cross-flow mode shape. Regardless of the symmetry of the cross-flow mode shape with respect to the center of the cylinder, the in-line drag force fluctuations are symmetrically distributed. Therefore, the in-line modal force for all even-numbered modes is zero. In this example, although the drag force fluctuations were at the natural frequency of the fourth in-line mode (an antisymmetric mode), the dominant modal force corresponded to the third mode (a symmetric mode), resulting in non-resonant third mode motion [10].

Similar peculiar results of non-resonant, in-line motion also happened under non-lock-in conditions and can be explained with an understanding of the quadratic relationship between in-line and cross-flow response.

BISPECTRAL ANALYSIS OF QUADRATIC CORRELATION

From the results of modal analysis there was substantial evidence of a quadratic relationship between in-line and cross-flow response. Higher order spectral analysis was required to study the correlation between time-histories resulting from a non-linear process. The bispectrum was used here to investigate the quadratic coupling between response in the cross-flow and in-line directions [10]. General information on non-linear spectral analysis may be found in References [14]–[17].

For a stationary random time series $x(t)$ the auto-bispectrum, $B(\omega_j, \omega_k)$, of $x(t)$ is defined as:

$$B_{xxx}(\omega_j, \omega_k) = E[X_j X_k X^*_{j+k}], \tag{12}$$

where ω_j and ω_k are discrete frequencies at which a Fourier transform has been computed. X_j and X_k are the Fourier transform coefficients computed from the time series $x(t)$ at frequencies ω_j and ω_k, and X^*_{j+k} is the complex conjugate of the coefficient at ω_{j+k}. $E[\ ]$ is the expectation operator and is computed as an ensemble average. The mathematical definition of the Fourier transform used is

$$X_k = \frac{1}{T}\int_0^T x(t) \exp(i\omega_k t)\, dt. \tag{13}$$

In this paper the bispectrum calculations were made in the following way. A stationary time series was sampled at 30 Hz. Fast Fourier transforms of 100 segments, all 128 samples in length were computed. Ensemble averages using the 100 realizations were used to compute each bispectrum point. The frequency resolution is therefore 0·23 Hz and the maximum frequency in the spectrum is 15 Hz. The results are more easily understood when plotted as coherence functions.

The auto-bicoherence spectrum, a normalized auto-bispectrum is

$$b_{xxx}(\omega_j, \omega_k) = \frac{|B_{xxx}(\omega_j, \omega_k)|}{\{E[|X_j X_k|^2]E[|X^*_{j+k}|^2]\}^{1/2}}. \tag{14}$$

By using Schwarz's inequality, it can be shown that the auto-bicoherence spectrum is bounded by 0 and 1. If the component at $\omega_j+\omega_k$, is related by non-linear quadratic coupling the auto-bicoherence spectrum will be close to unity. On the other hand, if the component at $\omega_j+\omega_k$ is uncorrelated quadratically to the components at ω_j and ω_k, the auto-bicoherence will be near zero. For this application, the cross-bispectrum between two time series $x(t)$ and $y(t)$ is the most useful.

Let $x(t)$ and $y(t)$ be two zero-mean jointly stationary time series; then the cross-bispectrum between $x(t)$ and $y(t)$ is

$$B_{xxy}(\omega_j, \omega_k) = E[X_j X_k Y^*_{j+k}]. \tag{15}$$

The cross bicoherence spectrum between $x(t)$ and $y(t)$ is

$$b_{xxy}(\omega_j, \omega_k) = \frac{|B_{xxy}(\omega_j, \omega_k)|}{\{E[|X_j X_k|^2]E[|Y^*_{j+k}|^2]\}^{1/2}}. \tag{16}$$

The cross bicoherence spectrum also ranges from zero to unity. Bicoherence functions require three dimensional plots, one axis each for frequencies ω_j and ω_k and a magnitude axis.

Lock-in Example

Figures 4 and 6 show the acceleration spectra for cross-flow and in-line motion under lock-in conditions. The principal cross-flow peak occurs at 2·4 Hz and the principal in-line response peak occurs at 4·8 Hz. The cross-bicoherence for this case, Figure 17, has its highest peak at frequencies $(f_j, f_k) = (2{\cdot}4$ Hz, 2·4 Hz). These figures are presented showing frequencies on two axes. The height is to be interpreted as resulting from moving the base of any peak of interest down to the horizontal axis and then estimating the peak height on the vertical scale of zero to 1·0, shown at the left of the figure. The vertical frequency axis goes from 0 to 7·5 Hz as shown on the right of the figure. Therefore, peak X has a height of 1, and corresponds to a sum frequency of 2·4 Hz + 2·4 Hz = 4·8 Hz. This essentially perfect coherence is the result of a quadratic relationship between the 2·4 Hz vibration energy in the cross-flow motion and the 4·8 Hz motion in-line.

Non-lock-in Example

Figures 8 and 9 show cross flow and in-line response spectra under non-lock-in conditions. The cross-bicoherence for this case is given in Figure 18. The peaks labeled X, Y and Z demonstrate the quadratic coherence between peaks E, F and G in the in-line spectrum and peaks A, B, C and D in the cross-flow spectrum. For example, the peak E at 3·70 Hz in the in-line spectrum occurs at the sum of frequencies at A and B (1·70 + 2·00 Hz). The quadratic relationship is confirmed in peak X in Figure 18 which is

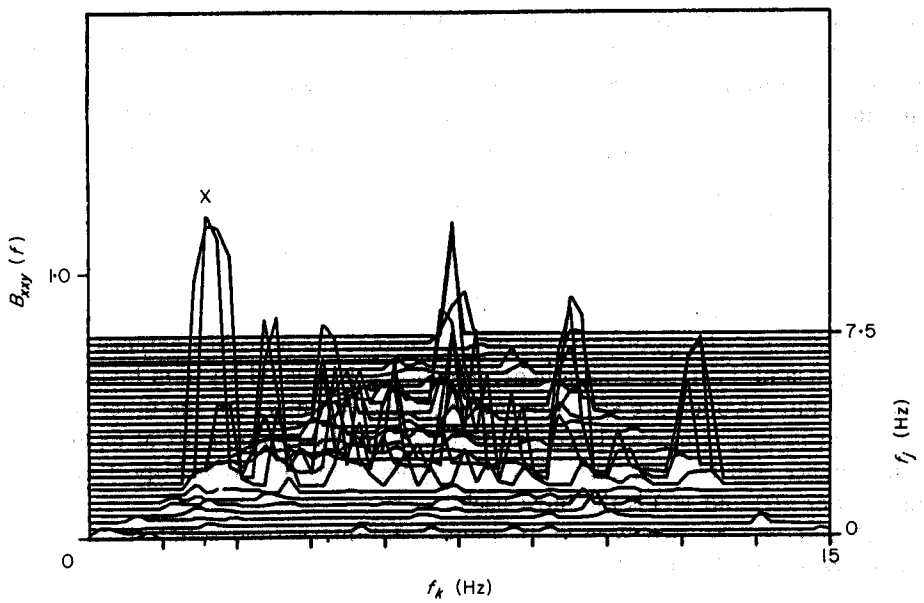

Figure 17. Cross-bicoherence between cross-flow and in-line response at lock-in. Frequencies: $X = (f_A, f_A) = (2{\cdot}4, 2{\cdot}4)$.

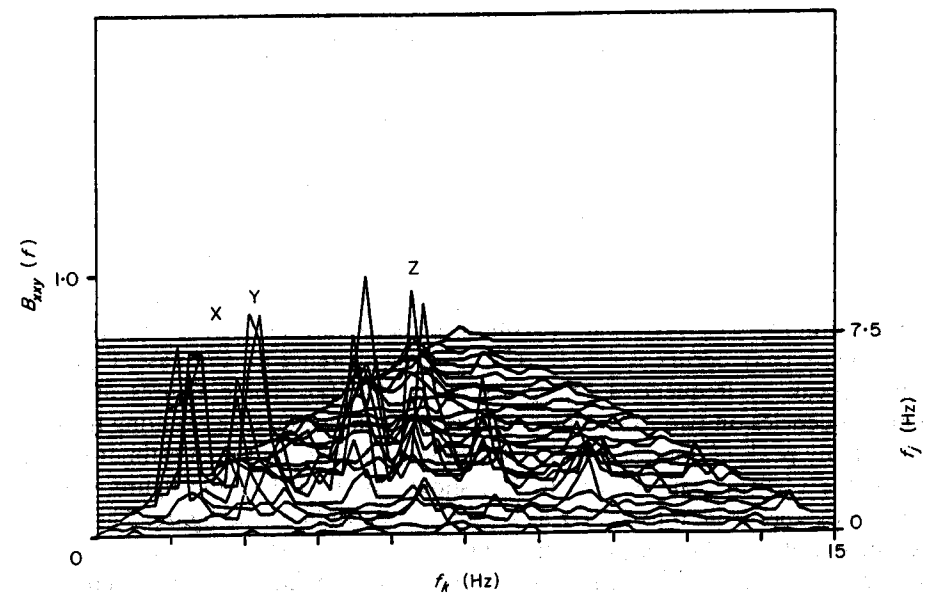

Figure 18. Cross-bicoherence between cross-flow and in-line response at non-lock-in. Frequencies: $X = (f_A, f_B) = (1{\cdot}70, 2{\cdot}00)$, $f_E = f_A + f_B$. $Y = (f_A, f_C) = (1{\cdot}70, 3{\cdot}20)$, $f_F = f_A + f_C$. $Z = (f_A, f_D) = (1{\cdot}70, 6{\cdot}40)$, $f_G = f_A + f_D$.

at $(f_j, f_k) = (1{\cdot}7, 2{\cdot}0\,\text{Hz})$ and is near 0·6 in height. Other similar correlations are specifically indicated in the Figure.

Sheared Current Example

The bispectrum results shown so far are for the uniform flow, low modal density data obtained at Castine. To investigate the extent to which the hypothesis of quadratic

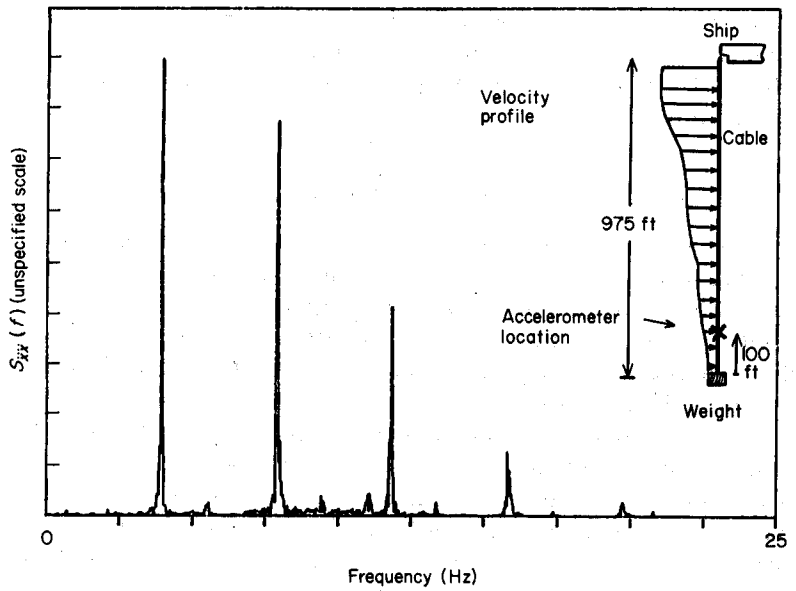

Figure 19. Linear spectrum of acceleration response from the Arctic experiment.

correlation can be generalized, a much different data set was needed. The Arctic experiments conducted by Vandiver and Kim were in sheared flows, using cables which were long enough to have flow-induced vibration properties characteristic of infinitely long cables [8, 9].

The test cable, 975 ft (297 m) in length, in this example, was suspended vertically from a research vessel with a heavy weight at the bottom end. An accelerometer was located at 100 ft (30·5 m) from the bottom end of the cable, orientated at an unknown angle to the flow. The measured response had both in-line and cross-flow response components in it. Figure 19 shows on a linear scale the FFT power spectrum of the measured response with

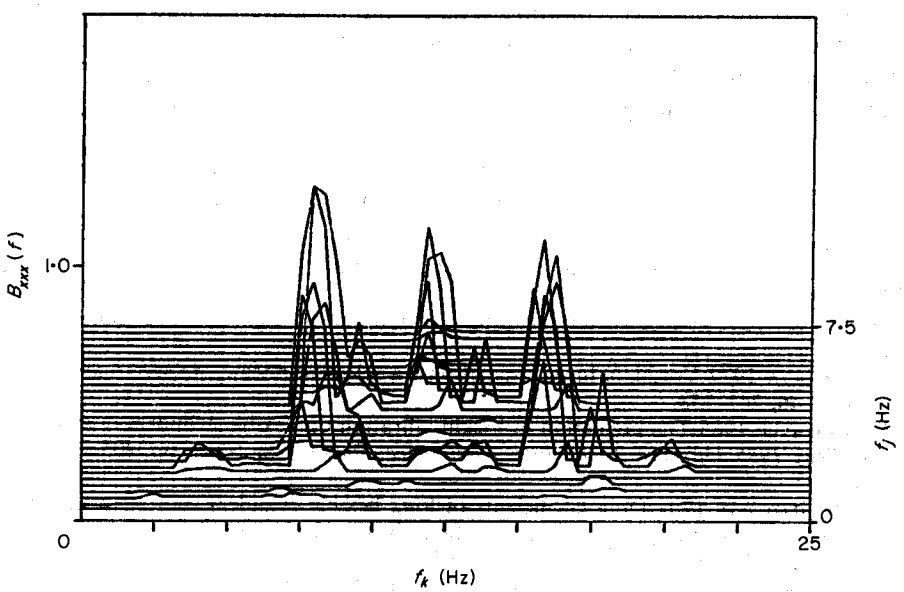

Figure 20. Auto-bicoherence of single-axis acceleration data from the Arctic experiment.

peaks at 4, 8, 12 and 16 Hz. Figure 20 shows the auto-bicoherence for these data revealing numerous peaks of high coherence. The most notable one is at $(f_j, f_k) = (8{\cdot}0, 4{\cdot}0\ \text{Hz})$, thus demonstrating that quadratic correlation exists even in a long cable, with sheared flow.

CONCLUSIONS

A variety of field vibration data has been used to demonstrate that for all conditions studied including lock-in, non-lock-in, uniform and sheared flow, quadratic correlation exists between in-line and cross-flow vibration components.

These results suggest that the time series modeling or prediction of the vibration response of marine risers, cables, pipelines and other cylinders exposed to currents should take into account these non-linear correlations. This is especially true when fatigue damage prediction is a concern, because fatigue is dependent on stress statistics and these depend on the correlation between various vibration components.

When estimating stress statistics for mechanical systems, it is desirable and often assumed that the stress-time histories can be modeled as Gaussian random processes. It is a mathematical fact that if the bispectrum of a time series is non-zero, the time series is not the result of a Gaussian or normally distributed random process. It is not appropriate to model flow-induced vibration as a Gaussian random processes.

This paper has demonstrated strong quadratic correlation between cross-flow and in-line vibration caused by vortex shedding. This suggests that it should be possible to identify the second-order non-linear transfer function which can relate the cross-flow to the in-line vibration. In other words, given the cross-flow time series and the proper non-linear transfer function, one should be able to model or predict the resulting in-line vibration. This has been done by the authors and is presented in References [10, 12].

ACKNOWLEDGEMENTS

This research represents a segment of a multi-year program at M.I.T. focused on the understanding of flow-induced vibration. The overall program has had broad federal and industrial support. This particular portion was sponsored by the Technology Assessment and Research Branch of the Minerals Management Service and by the Marine Technology Division of the (United States of America) Naval Research Laboratory.

REFERENCES

1. O. M. GRIFFIN and S. E. RAMBERG 1982 Some recent studies of vortex shedding with application to marine tubulars and risers. *ASME Journal of Energy Resources Technology* **104,** 2–13.
2. R. KING 1977 A review of vortex shedding research and its application. *Ocean Engineering* **4,** 141–171.
3. T. SARPAKAYA 1979 Vortex-induced oscillations, a selective review. *ASME Journal of Applied Mechanics* **46,** 241–258.
4. J. K. VANDIVER 1985 The prediction of lockin vibration on flexible cylinders in a sheared flow. *Proceedings 1985 Offshore Technology Conference*, Paper No. 5006, pp. 405–412, Houston, Texas.
5. J. C. MCGLOTHLIN 1981 Drag coefficients of long flexible cylinders subject to vortex-induced oscillation. S.M. Thesis presented to the Massachusetts Institute of Technology, Cambridge, Massachusetts, U.S.A.
6. J. K. VANDIVER 1983 Drag coefficients of long flexible cylinders. *Proceedings 1983 Offshore Technology Conference*, Paper No. 4490, pp. 405–414, Houston, Texas.

7. O. M. GRIFFIN and J. K. VANDIVER 1984 Vortex-induced strumming vibrations of marine cables with attached masses. *ASME Journal of Energy Resources Technology* **106,** 458–465.
8. Y.-H. KIM 1984 Vortex-induced response and drag coefficients of long cables in ocean currents. Ph.D. Thesis, Department of Ocean Engineering, Massachusetts Institute of Technology, Cambridge, Massachusetts, U.S.A.
9. Y.-H. KIM, J. K. VANDIVER and R. HOLLER 1985 Vortex-induced vibration and drag coefficients of long cables subjected to sheared flows. *Proceedings 4th International Offshore Mechanics and Arctic Engineering Symposium*, pp. 584–592. New York: ASME.
10. J.-Y. JONG 1984 The quadratic correlation between in-line and cross-flow vortex-induced vibration of long flexible cylinders. Ph.D. Thesis, Department of Ocean Engineering, Massachusetts Institute of Technology, Cambridge, Massachusetts, U.S.A.
11. R. B. CAMPBELL and J. K. VANDIVER 1982 The determination of modal damping ratios from maximum entropy spectral estimates. *ASME Journal of Dynamic Systems, Measurement and Control* **104,** 78–85.
12. J.-Y. JONG and J. K. VANDIVER 1985 The identification of the quadratic system relating cross-flow and in-line vortex-induced vibration. In *Dynamic Systems Measurement and Control*, ASME 1985 Winter Annual Meeting.
13. L. MEIROVITCH 1967 *Analytical Methods in Vibrations*. New York: Macmillan.
14. D. R. BRILLINGER 1975 *Time Series*. New York: Holt.
15. D. R. BRILLINGER and M. ROSENBLATT 1967 Asymptotic theory of estimation of kth order spectra. In *Spectral Analysis of Time Series* (ed. B. Harris). New York: Wiley.
16. Y.-C. KIM and E. J. POWERS 1979 Digital bispectral analysis and its application to nonlinear wave interactions. *IEEE Transactions on Plasma Science* **PS7**, 120–131.
17. Y.-C. KIM, W.-F. WANG, E. J. POWERS and J. R. ROTH 1979 Extension of the coherence function to quadratic models. *Proceedings of the IEEE* **67,** 428–429.